Capture and detection of SO_2 by a chemically stable Mg(II)-MOF

Eva Martínez-Ahumada,[†a] Dae won Kim,[†b] Mohammad Wahiduzzaman,[†c] Paulina Carmona-Monroy,[a] Alfredo López-Olvera,[a] Daryl R. Williams,[d] Vladimir Martis,[e] Hugo A. Lara-García,[f] S. López-Morales,[g] Diego Solis-Ibarra,[a] Guillaume Maurin[*,c] Ilich A. Ibarra[*,a] and Chang Seop Hong[*,b]

[a.] *Laboratorio de Fisicoquímica y Reactividad de Superficies (LaFReS), Instituto de Investigaciones en Materiales, Universidad Nacional Autónoma de México, Circuito Exterior s/n, CU, Coyoacán, 04510, Ciudad de México, Mexico.*
[b.] *Department of Chemistry, Korea University Seoul 02841, Republic of Korea.*
[c.] *ICGM, Univ. Montpellier, CNRS, ENSCM, Montpellier, 34293, France.*
[d.] *Director of Discovery Space and Professor of Particle Science, Department of Chemical Engineering, Imperial College, Kensington, London SW7 2BY, U.K.*
[e.] *Surface Measurement Systems, Unit 5, Wharfside, Rosemont Road, London HA0 4PE, U.K.*
[f.] *Instituto de Física, Universidad Nacional Autónoma de México, Circuito de la Investigación Científica s/n, CU, Coyoacán, Ciudad de México, Mexico.*
[g.] *Instituto de Investigaciones en Materiales, Universidad Nacional Autónoma de México, Circuito Exterior s/n, CU, Del. Coyoacán, Ciudad de México, México*
* Corresponding Authors
E-mail: argel@unam.mx, guillaume.maurin1@umontpellier.fr and cshong@korea.ac.kr, Fax: +52(55) 5622-4595.

Synthesis

Mg_2(dobpdc) was synthesized according to the literature with a slightly modified procedure.[1] Into a 32 mL Pyrex cell, H_4dobpdc (263.14 mg, 0.959 mmol, 1 eq), $MgBr_2 \cdot 6H_2O$ (841.11 mg, 2.878 mmol, 3 eq), and 12 mL of solvent (DMF:EtOH = 1:1 (v:v)) were loaded and sonicated until clear solution obtained. The Pyrex cell was sealed with a PTFE cap and the solution was irradiated in a microwave reactor (CEM Discover) for 20 min at 403 K. After the solution was cooled to room temperature, the MOF solid was collected with filtration and wash with excess DMF and methanol. The collected MOF solid was immersed in DMF and heated at 333 K overnight. The washed MOF solid was collected via filtration and re-immersed in methanol to exchange solvent for 3 days. In each day, the supernatant was decanted and fresh methanol was added. Elemental analysis (%) calculated for $[Mg_2(dobpdc)(MeOH)1.5(H_2O)_{0.5}] \cdot 2.1H_2O$: C 44.78, H 4.66; found: C 44.66, H 4.29. Before gas sorption, Mg_2(dobpdc) was activated under high vacuum at 523 K for 24 h. Yield = 284.3 mg (93%).

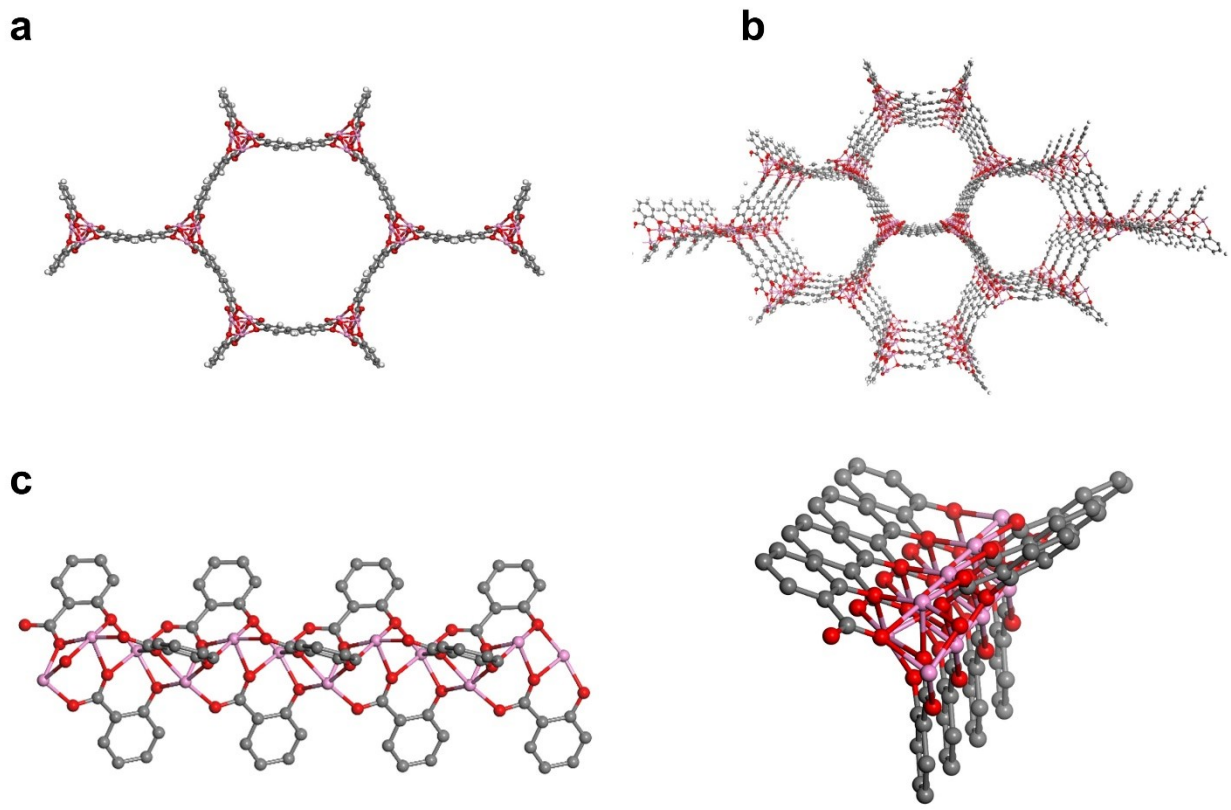

Figure S1. (a) The structure of Mg_2(dobpdc) MOF material as viewed down the c-axis. (b) View of structure of Mg_2(dobpdc) complex with one dimensional hexagonal channels. (c-d) View of the Mg nodes, hydrogen atoms are omitted for clarity. Color code: carbon (light gray); oxygen (red); magnesium (magenta).

Powder X-ray diffraction Experiments

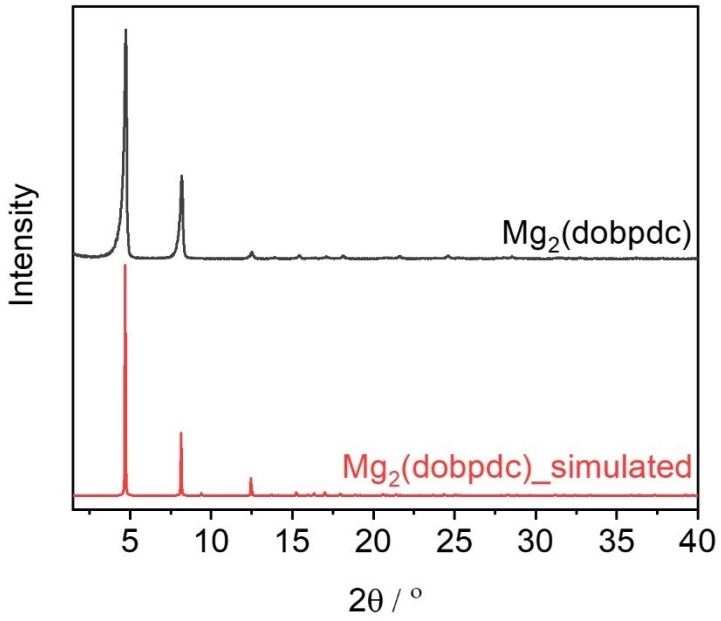

Figure S2. Powder X-ray diffraction patterns of Mg_2(dobpdc) simulated (red line) and after solvent exchange (black line).

IR spectroscopy Experiments were recorded with the attenuated total reflectance (ATR) module by using a Nicolet iS10 FTIR spectrometer.

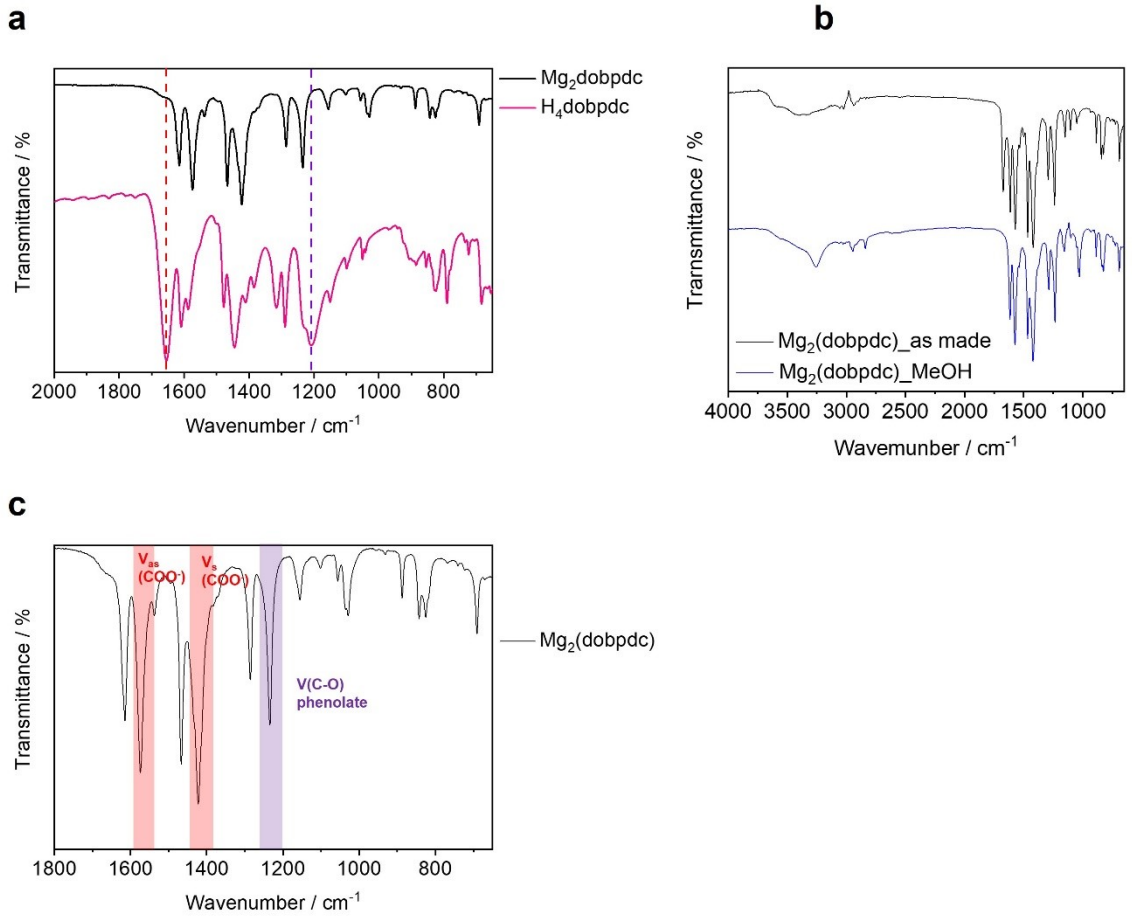

Figure S3. IR spectra of Mg_2(dobpdc) (a) IR spectra of Mg_2(dobpdc) and H_4dobpdc. (b) The black and blue lines represent as-made and solvent-exchanged. (c) IR peaks related to the coordination between ligand and metal in Mg_2(dobpdc).

Thermogravimetric analysis

Thermogravimetric analyses (TGA) were performed with a ramp rate of 2 °C min^{-1} up to 900 °C in an N_2 (99.999%) flow using a TA instruments Discovery TGA.

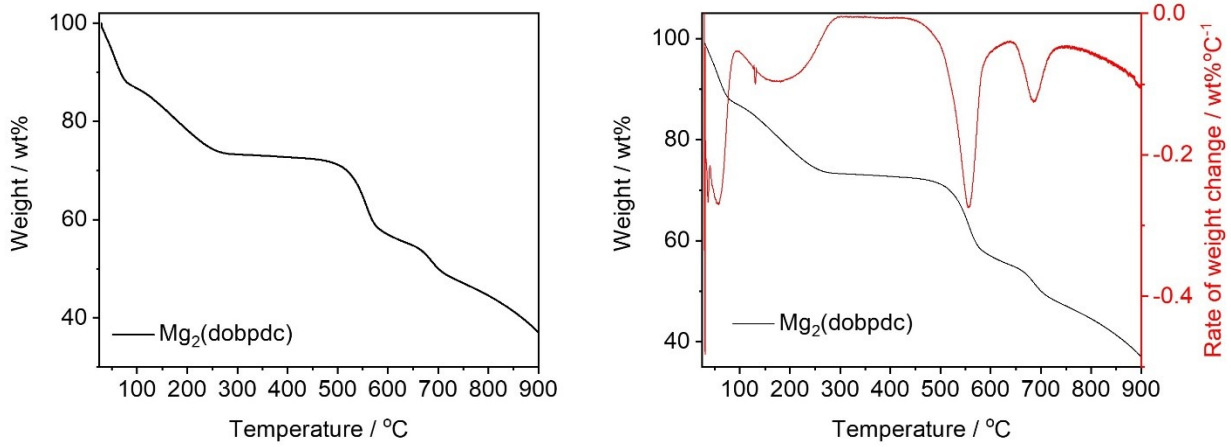

Figure S4. Thermogravimetric analysis of solvent-exchanged Mg_2(dobpdc) (left panel). Differentiated thermogravimetric analysis data (right panel).

Gas sorption measurements

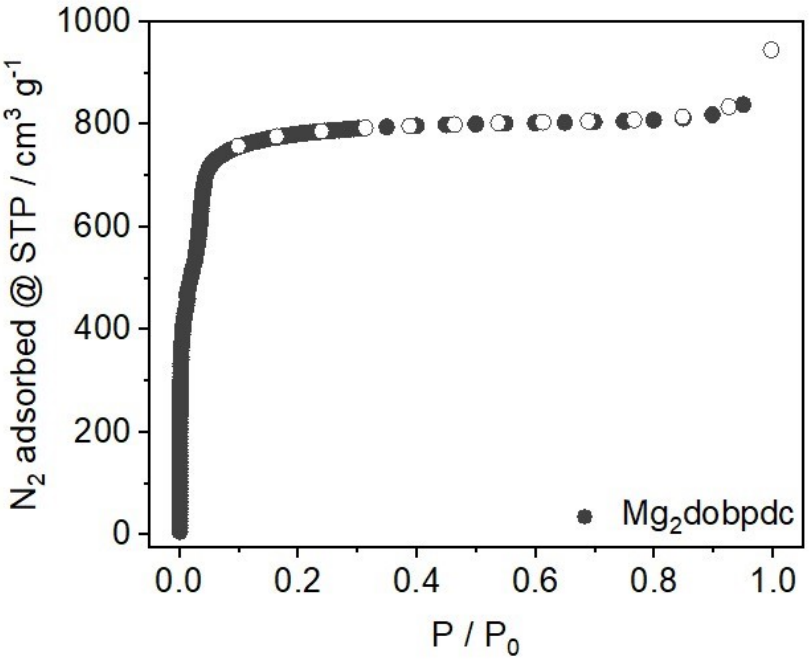

Figure S5. N_2 isotherm of the pristine Mg_2(dobpdc) MOF material at 77 K. The closed circle represents adsorption, and the open circle represents desorption.

Pore size distribution of Mg_2(dobpdc)

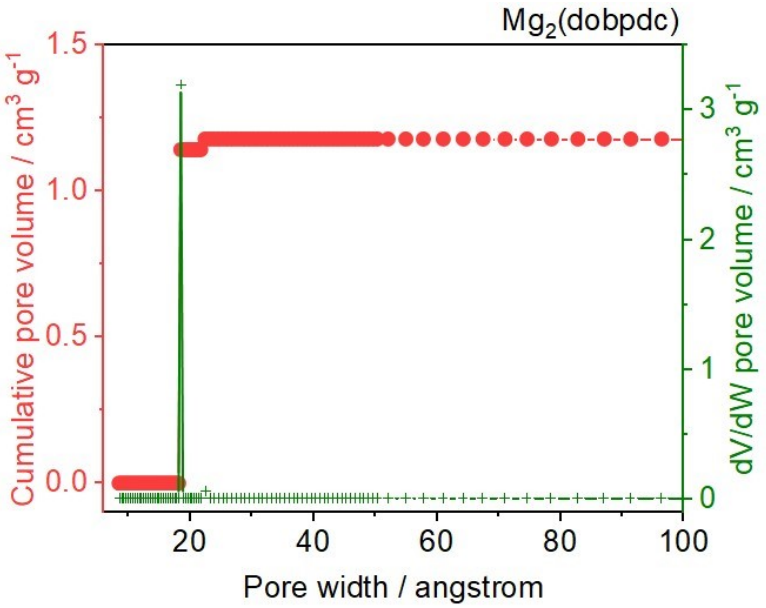

Figure S6. DFT pore size distribution and NLDFT fitting of Mg_2(dobpdc). The pore size distribution was analyzed with N_2-cylindrical pore-oxide surface model.

Determination of Lewis Acidic sites by CO Infrared Spectroscopy

Carbon monoxide (CO) is a commonly used to probe molecule for Lewis acidity.[2] A Lewis acid interaction with the carbon electron lone pair of CO leads to a withdraw of electron density from the antibonding σ orbital, resulting in an IR peak shifting to higher energies compared to the CO gas phase.[3]

DRIFTS experiments were performed using an environmentally controlled PIKE DRIFTS cell with ZnSe windows coupled to a Thermo Scientific Nicolet iS50 spectrometer with a MCT/A detector. Absorbance spectra were obtained by collecting 64 scans at a 4 cm^{-1} resolution. A sample of 0.020 g was pre-treated

in situ under a He flow at 523.15 K for 4 h. After this treatment, the sample was cooled to room temperature and then, a flow of carbon monoxide (CO: 30 mL min^{-1}; 5 % of CO diluted in He) was passed through the sample. Figure S7a shows the spectra of CO adsorption (298 K) measured at different times of CO sorption (min) on an activated sample of Mg_2(dobpdc).

From a qualitative point of view, the ν(CO) band at ~2207-2170 cm^{-1} highlight the formation of CO species bonded to coordinatively unsaturated metal sites (CUS). The location of this band depends on the metal centre in MOF structure. In the M-MIL-100 family (M = Al, Fe, and Cr) the wavenumber of CO probe molecule is observed at 2195-2184 cm^{-1};[4] 2192-2173 cm^{-1};[5] and 2215-2180 cm^{-1},[6] respectively. While in the case of MIL-101(Cr)-4F(1%) this band was observed at 2191 cm^{-1}.[7] In our case, after only 1 min of CO exposure, we observe a band at 2181 cm^{-1} with a shoulder near 2178 cm^{-1} and 2173 cm^{-1} (Figure S7b, purple spectra). With the introduction of large amounts of CO, i e. more exposure time, the ν(CO) band is shifted first to 2179 cm^{-1} (Figure S7b, blue spectra), and then to 2178 cm^{-1} with a shoulder near 2173 cm^{-1} (Figure S7b, green spectra). In line with the previously observed cation-dependent vibrational band,[8] this band is attributed to CO interacting with the Lewis Mg^{2+} sites, corroborating that the Mg^{2+} are accessible open metal sites. This low frequency band should correspond to the more stable CO: Mg^{2+} species, as the early observed in MIL-100(Fe) material.[5] Additionally, the intensity of ν(CO) increases over time two-fold from 1 minute to 5 minutes of CO exposure. In addition to the bands discussed above, it is possible to observe bands at 2160-2115 cm^{-1} which corresponds to physisorbed species of CO, see Figure S7c. Therefore, we should conclude that the preferential bonding sites in Mg_2(dobpdc) MOF is the Mg^{2+} CUS which pave the ways towards their uses for a preferential adsorption of SO_2.

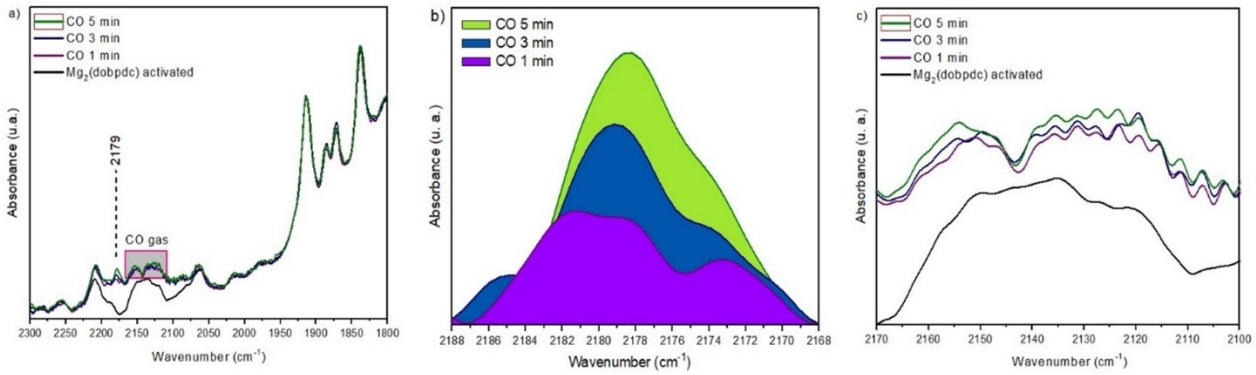

Figure S7. In situ DRIFTS spectroscopy spectra of CO adsorbed at different times over activated Mg_2(dobpdc) at 298 K, a) in the region between n 2300 and 1800 cm^{-1}. b) in the region between n 2188 and 2168 cm^{-1}. c) in the region between n 2170 and 2100 cm^{-1}.

Sulfur dioxide capacities of reported adsorbents

Table S1. List of SO_2 capacities of reported adsorbents.

Material	SO_2 capacity [mmol g^{-1}]		Pore Volume [cm^3 g^{-1}]	Packing Density [g cm^3]	Reference
	at 0.1 bar	at 1 bar			
*FMOF-2		2.2			9
MFM-305	6	7	0.37	1.2	10
MFM-300(Al)		7.1	0.38	1.21	11
MIL-160	5.5	7.2[a]	0.46	1.0	12
*MIL-101(Cr)-NH_2	~2.2[b]	7.3a	1.34	0.35	13
MFM-300(In)	7.5	8.28	0.42	1.26	14
MFM-300(Sc)	8	9.4	0.58	1.04	15
Ni(bdc)(ted)0.5	4.5	9.97	0.67	0.96	16
MOF-808	~2.0[b]	9.99	0.696	0.919	17
MFM-202a	3	10.2	0.95	0.69	18

MOF-808-His	5.2	10.36	0.5223	1.26	19
MIL-125(Ti)-NH_2[a]	7.9	10.8	0.65	1.06	12
SIFSIX-1-Cu	8.7	11	0.68	1.04	20
ECUT-111	6.4	11.6	0.63	1.18	21
Fe-soc-MOF	6.5	11.7	0.8	0.94	22
NU-1000	2.6	12.2	1.196	0.65	23
MFM-601	4.13	12.3	1.5	0.53	24
*HKUST-1[a]	10.1	13.8	0.612	1.44	25
MOF-808	3.6	14.6a	0.749	1.24	26
MIL-100(Al)	2.5	16.3	0.824	1.27	26
*MIL-101(Cr)-NH_2[a]	4.1	16.7	1.162	0.92	27
*CB6@MIL-101-Cl	2	17.0	1.0	1.08	26
*MIL-101(Al)-NH_2	3.6	17.3	1.001	1.11	26
*MFM-170	7	17.5	0.88	1.27	12
*MIL-101(Cr)-4F(1%)	4.9	18.4	1.19	0.99	7
*MOF-177	1.3	25.7[a]	1.51	1.09	12
***Mg_2(dobpdc)**	**7.4**	**19.5**	**1.29**	**0.97**	**This work**
*Mg-MOF-74	~6.2[b]	8.6	0.78	0.71	28
*Mg-MOF-74		1.6[c]	0.78	0.02	29
Mg-gallate	6.7	7.61	0.2	2.46	30
MgO		2.49[d]			31

[*] Presence of open metal sites in the MOF. [a] Measured at 293 K. [b] Estimated from isotherm. [C] Breakthrough SO_2 capacity (SO_2 concentration = 375 ppm). [d] Breakthrough SO_2 capacity (SO_2 concentration = 50,000 ppm).

Computational details

Force Field Parameterization

The interactions between unlike force field centers were treated by means of the Lorentz-Berthelot combination rule. The remainder of the interaction, i.e., SO_2 – Mg(CUS) interactions were modeled with Morse potential. The decomposed energy terms along the approaching path offers a clear picture of the strength of the SO_2 – Mg (CUS) interactions. At this stage, the corresponding Morse potential parameters for the S(SO_2) – Mg(CUS) and O(SO_2) – Mg(CUS) pair wise interactions were determined with The General Utility Lattice Program (GULP[32]) by minimizing the difference between the DFT interaction energies and the force field derived energies along the approaching path. However, on the contrary to the SO_2 binding distance with dobpdc^{4-} ligand's bridging aryloxide μ-O atoms and connected C(sp3) atoms deduced from the DFT equilibrium geometry (see Figure S8), corresponding LJ- sigma parameters deduced from the combination of UFF and SO_2 force field tend to overestimate the repulsion term quite significantly. Thereby, we have re-fitted the LJ sigma parameters for these two specific cross-interactions O(SO_2)–O(aryloxide) and S(SO_2)– C(OC) as depicted in Figure S9. The DFT interaction energies and decomposed energy terms along the approaching path used in the fitting process are presented in Figure S9. The optimized Morse parameters for the pair wise interactions for the S–Mg (CUS) and O–Mg (CUS) are given in Table S4 and the remaining parameters are given S5.

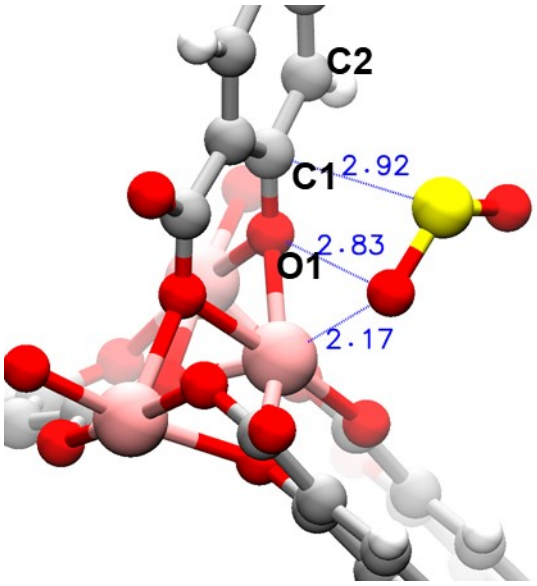

Figure S8. DFT optimized equilibrium configuration of SO_2–Mg_2(dobpdc) depicting dominant close contacts of SO_2 molecule with the framework atoms. O* and C* represent bridging aryloxide μ-O and connected C(sp3) atoms of the dobpdc^{4-} ligand, respectively.

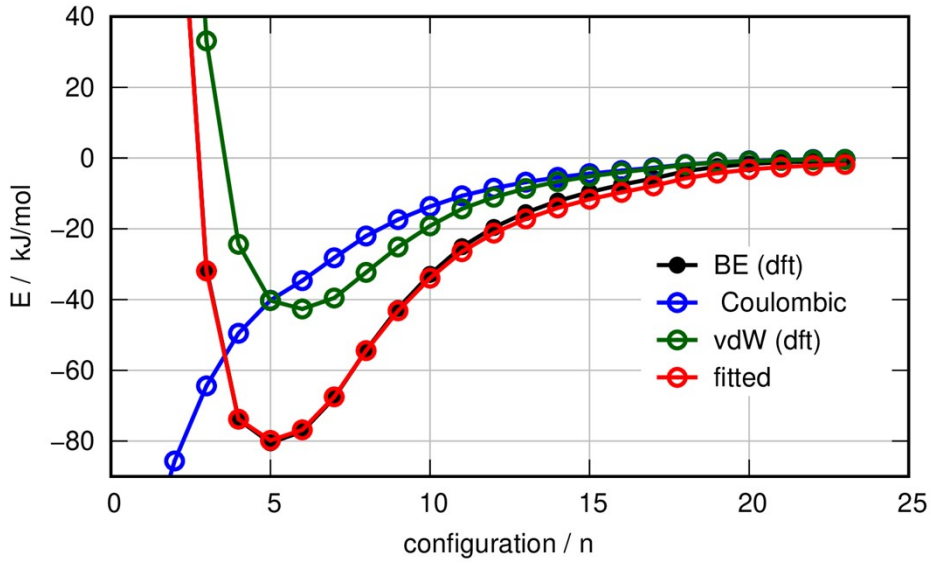

Figure S9. comparison of the DFT (rev-vdW-DF2) calculated binding energy curve of SO_2–Mg_2(dobpdc) framework interaction and the corresponding total interaction energies obtained from the fitted force field parameters.

Table S2. Intermolecular LJ-potential parameters for the SO_2 molecule taken from Sokolic et al.[33]

Pseudo atom type	**σ [Å]**	**ε/kB [K]**	**q [e]**
$S(SO_2)$	3.615	145.98	+0.470
$O(SO_2)$	3.005	57.50	-0.235

Table S3. LJ Potential parameters for the Mg_2(dobpdc) framework atoms.[34]

Atom type	**σ [Å]**	**ε/k_B [K]**
H	2.571	22.142
C	3.431	52.839
O	3.118	30.194

Table S4. DFT derived Morse potential parameters for the SO_2-Mg(CUS) interaction.

Pseudo atom pairs	**D_e [K]**	**a in [$Å^{-1}$]**	**r_o in [Å]**
$S(SO_2)$–Mg^{2+}	1403.5789	2.1369	3.5163
$O(SO_2)$–Mg^{2+}	1623.0321	2.0230	2.1927

Table S5. DFT derived LJ potential parameters for the SO_2- Mg_2(dobpdc) framework atoms.

Pseudo atom pairs	**σ [Å]**	**ε/k_B [K]**
S(SO2)– C1*	2.607	87.826
O(SO2)–O1*	2.524	41.667
*selected C and O atoms of the framework as indicated in Figure S8, for which LJ sigma parameters for the MOF-SO_2 cross interactions were re-fitted.		

Accessible surface area and pore volume calculation

The theoretical accessible surface areas (Sacc), pore volume of the geometric topology of the Mg_2(dobpdc) were calculated using zeo++ software.[35] A nitrogen sized (3.64 Å) probe molecule was used to calculate the accessible surface area. For the atoms of the MOF framework, default definition of the

atomic radii as recorded in the software was used. The free pore volume (Vpore) of the frameworks was calculated using the same geometric method but with a probe molecule of 0 Å.

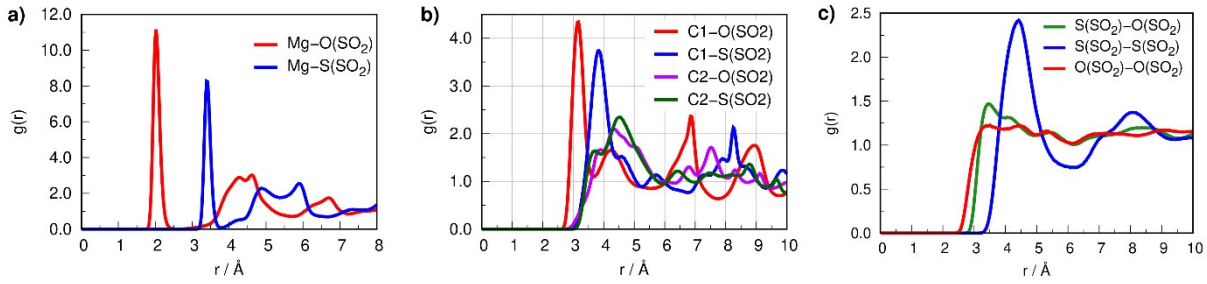

Figure S10. Intermolecular radial pair distribution functions of Mg_2(dobpdc) MOF surface atoms and adsorbed SO_2 molecules calculated at *P* = 0.10 bar (**a-b**), and guest SO_2 molecules with the same kind (**c**) calculated at *P* = 0.50 bar. C1 and C2 represent the carbons connected to aryloxide, and the C-H carbons of the dobpdc^{4-} ligand, respectively as depicted in Figure S8.

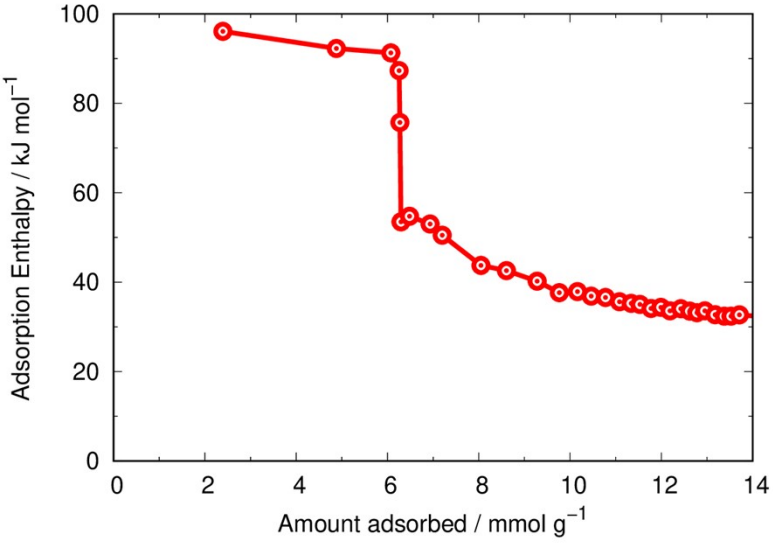

Figure S11. GCMC calculated adsorption enthalpies for SO_2 adsorption in Mg_2(dobpdc) MOF pore system.

Experimental Heat of Adsorption of SO_2

Additional 298 K and 308 K SO_2 adsorption isotherms were measured to estimate the heat of adsorption (Figure S12). A DSLF equation was used to fit the adsorption isotherms at low surface coverage, to estimate the heat of adsorption at zero coverage (Figure S13). The heat of adsorption at zero coverage was estimated in -29.86 kJ mol^{-1}.

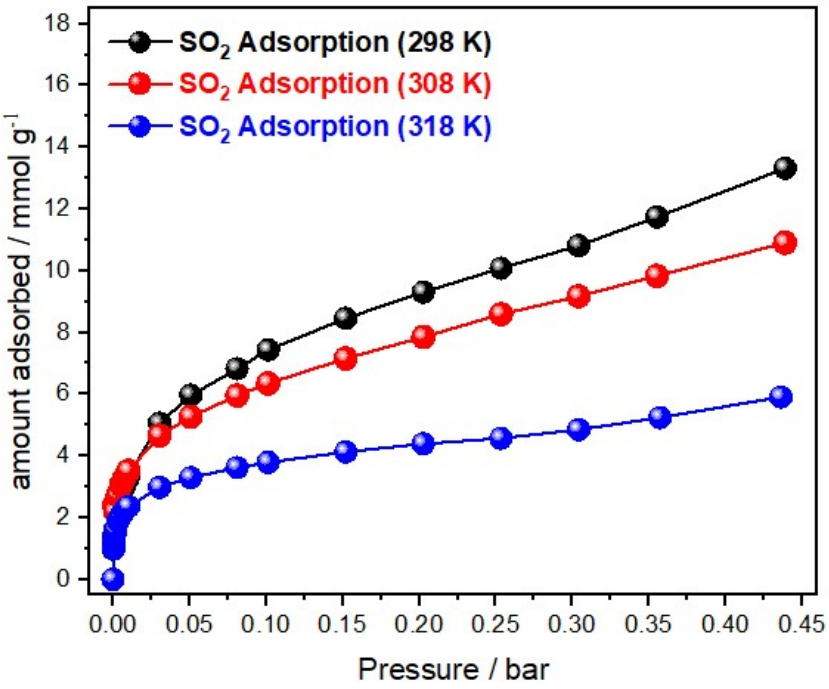

Figure S12. SO_2 adsorption isotherms of Mg_2(dobpdc) at 298, 308 and 318 K and up to 0.45 bar.

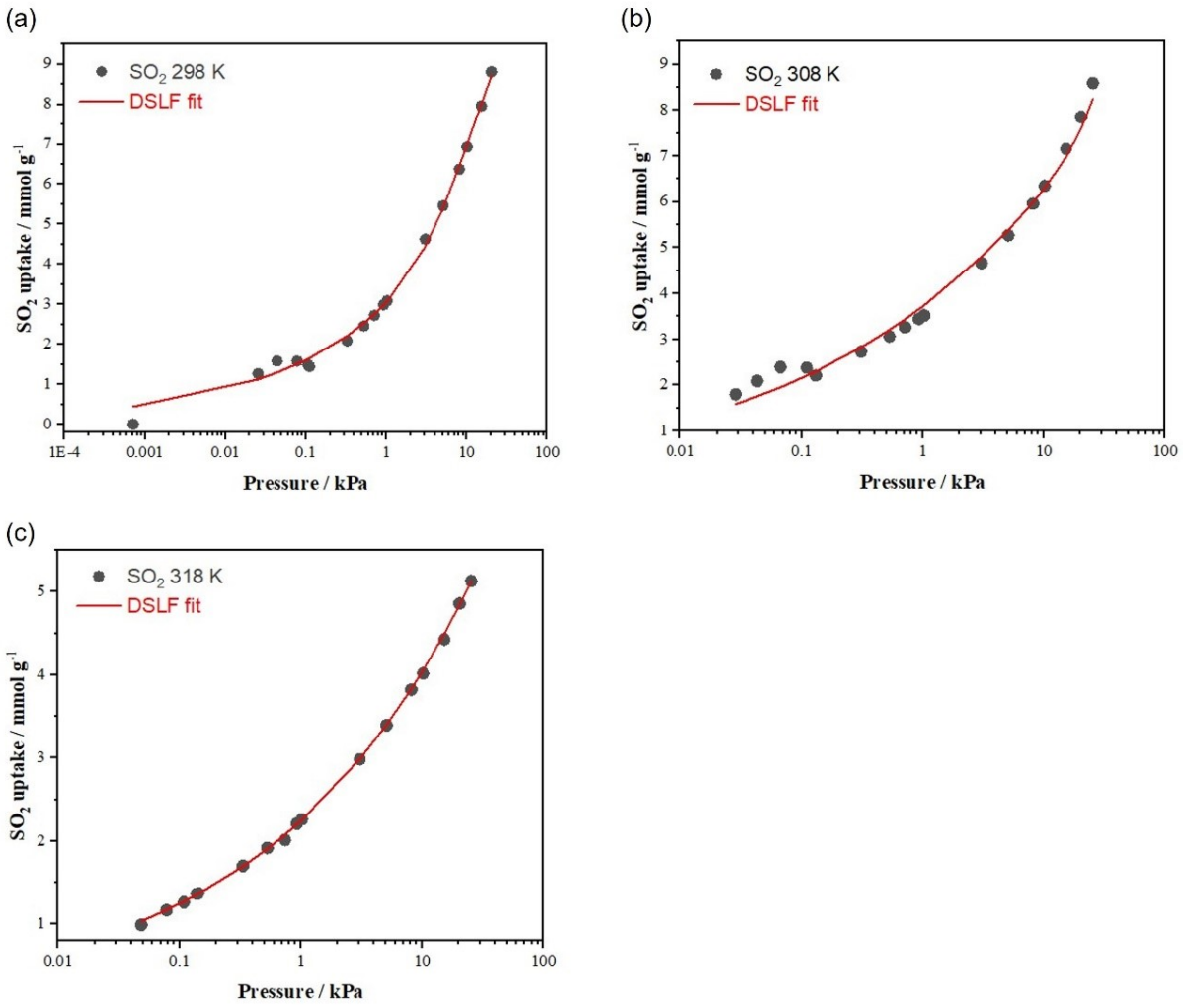

Figure S13. Dual site Langmuir Freundlich model (DSLF) fit of SO_2 isotherms in Mg_2(dobpdc) at (a) 298 K, (b) 308 K, and (c) 318 K.

SO_2 cycling experiments

The SO_2 cycling experiment was carried out using a Dynamic Gravimetric Gas/Vapour Sorption Analyser, DVS vacuum (Surface Measurement Systems Ltd). Mg_2(dobpdc) sample was degassed in vacuum vacuum (1 x 10^{-6} Torr) at 250 °C for 24 h. After cooling to 25°C, the first SO_2 isotherm was measured from 0.0007 to 100% P/P_0 of SO_2 gas, followed by the desorption isotherm. The same sample was then activated at identical conditions and adsorption-desorption SO_2 isotherm was measured. From the third isotherm, the

sample was activated only under vacuum (1 x 10^{-6} Torr) for 6 h, and the corresponding adsorption and desorption isotherms were measured until completing 50 cycles.

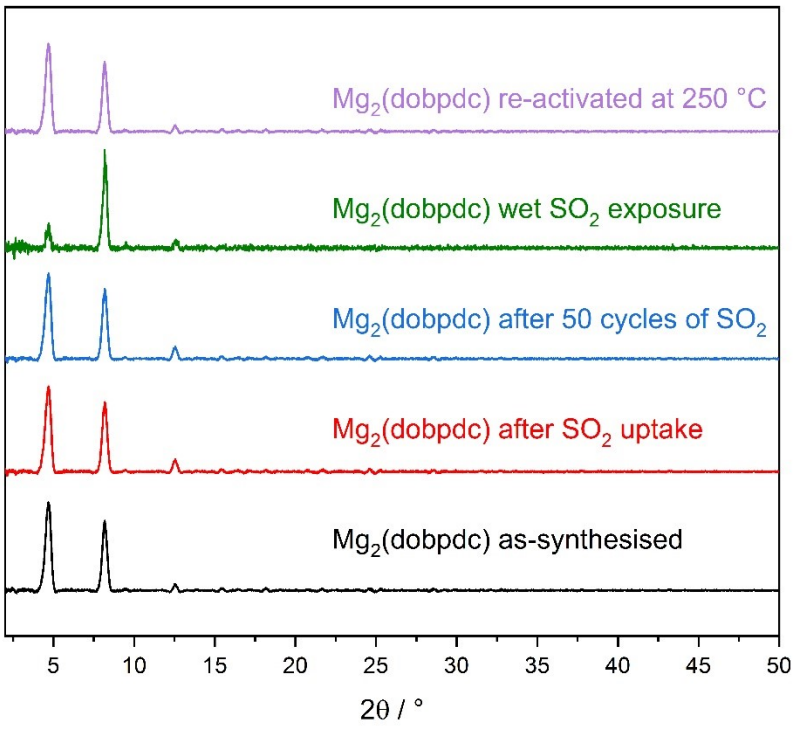

Figure S14. Powder X-ray diffraction patterns of Mg_2(dobpdc) after SO_2 adsorption experiments: as-synthesised (black line); after ads-des isotherm of SO_2 (red line); after 50 SO_2 adsorption cycles (blue line); and after wet SO_2 sorption (green line), the decrement of intensity on first peak is due to the presence of water molecules inside the pore.

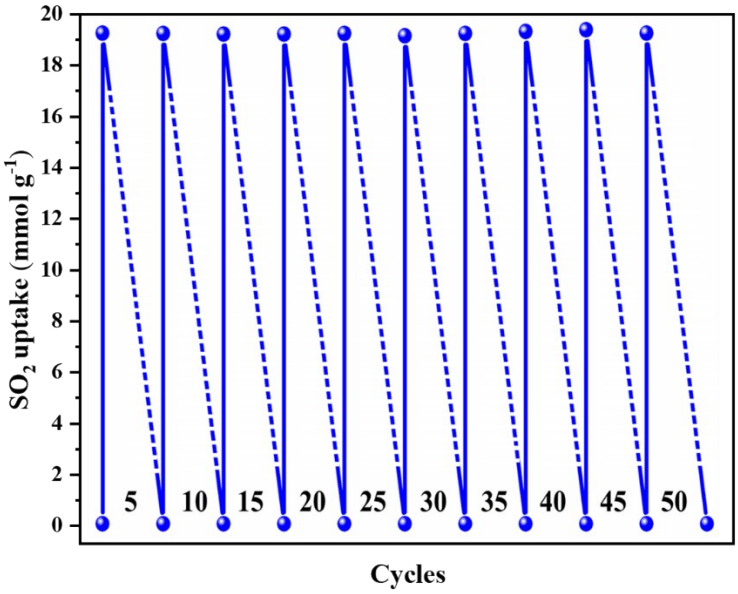

Figure S15. Ten adsorption–desorption cycles for SO_2 in Mg_2(dobpdc) at 298 K up to 1 bar (plotted every 5 cycles). The sample was activated at 250°C during 24 h under vacuum the two first cycles, from the third cycle the sample was active were under dynamic vacuum at 298 K between cycles, and no loss of uptake capacity was observed. Dashed lines represent the desorption isotherm.

Wet SO_2 exposure experiment

The system adapted from previously reported.[7] The system contains two principal parts: SO_2 gas generator (A) dropping funnel with H_2SO_4 conc. [1] connected to a Schlenk flask with Na_2SO_3 (s) under stirring [2]; and the saturation chamber (B), constructed from a round flask with distilled water [3], connected to a sintered glass filter adapter [4] and to a vacuum line [5]. First, 150 mg of the Mg_2(dobpdc) sample was activated in a sand bath at 250 °C under vacuum for 24 h, quickly placed on the glass adapter (powder bed of 1.5 mm) and the system was evacuated with a vacuum line. Next, SO_2 gas was generated by dripping concentrated sulfuric acid over Na_2SO_3, which passed through the sample continuously for 24 hours. The relative humidity of 60% was considered with and hygrometer inside the laboratory at the time of carrying out the experiment (not inside the home-designed setup). At this point, the relative humidity

inside the homemade device was not adequately controlled, as is the case in the experiment elegantly reported by C. Janiak *et al.* in 2021.[25]

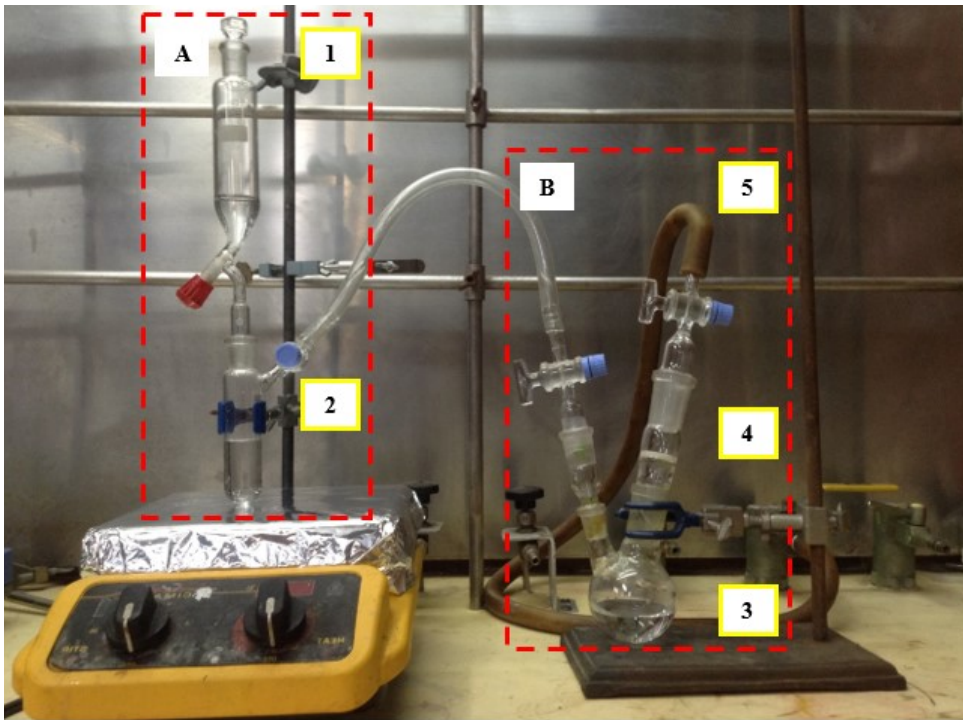

Figure S16. Homemade system for wet SO_2 adsorption experiments.

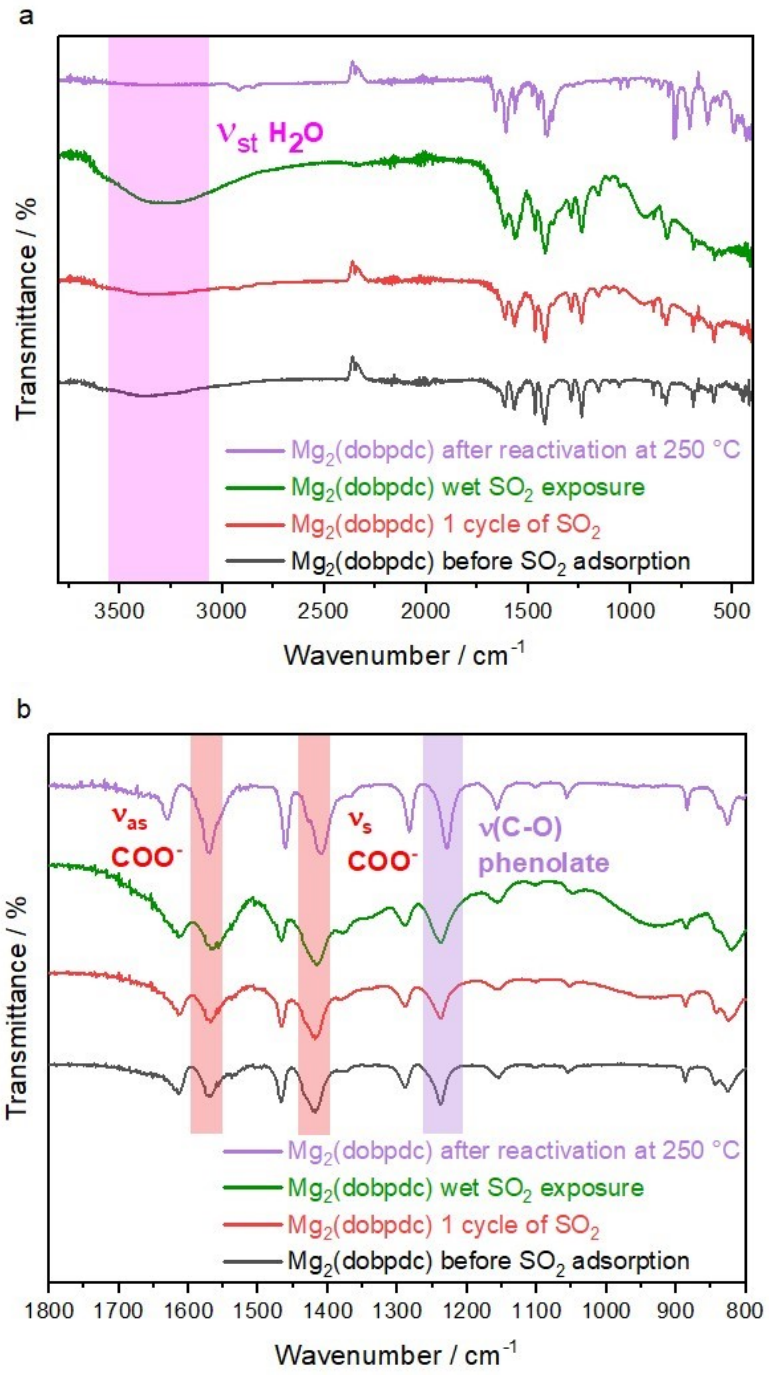

Figure S17. IR spectra of the pristine Mg_2(dobpdc) MOF material before and after exposure to dry and humid SO_2 gas. (a) IR broad peak related to the presence of H_2O in the framework after the SO_2/H_2O exposure (green spectra). (b) IR peaks related to the coordination between ligand and metal in Mg_2(dobpdc).

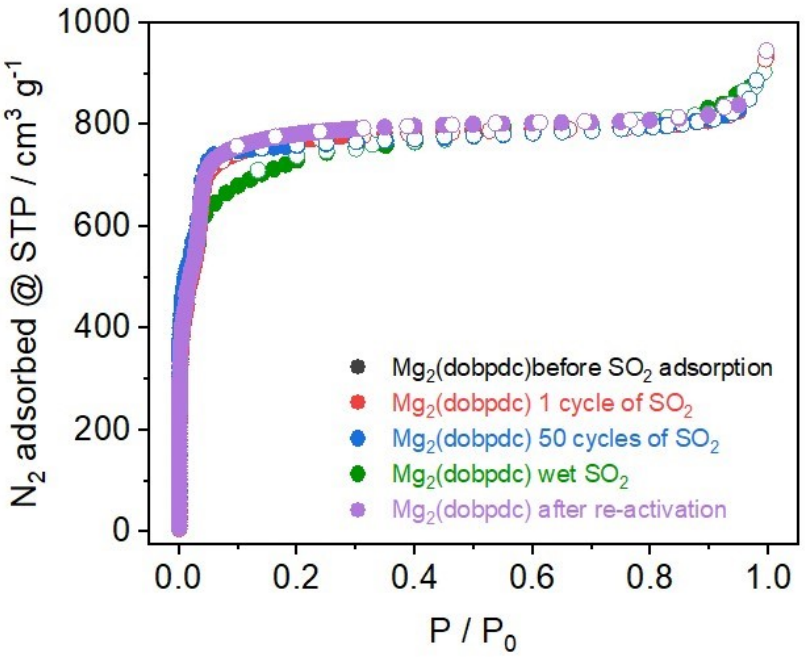

Figure S18. N_2 isotherms of the pristine Mg_2(dobpdc) MOF material before and after exposure to dry and humid SO_2 gas.

IAST Selectivity

Calculation of IAST selectivity

The IAST selectivities for SO_2/N_2 and SO_2/CO_2 at 298 K were calculated according to the ideal adsorbed solution theory (IAST).[36] To evaluate the sorption performance of Mg_2(dobpdc) for the separation of a binary mixed system, single-component isotherms were fitted to a Dual Site Langmuir Freundlich model (DSLF):

$$n(P) = \frac{a_1(b_1P)^{C_1}}{1+(b_1P)^{C_1}} + \frac{a_2(b_2P)^{C_2}}{1+(b_2P)^{C_2}}$$

where n is the gas adsorbed in mmol g^{-1}, P is the pressure in kPa, a is the maximal loading in mmol g^{-1}, b is the affinity constant in kPa^{-c}, and c is the heterogeneity exponent.

The adsorption selectivity for the binary mixture is defined as:

$$S_{i,j} = \frac{\frac{x_i}{yi}}{\frac{x_j}{y_j}}$$

where x is the mole fraction of components in the adsorbed phase and y is the gas mole fraction of components.

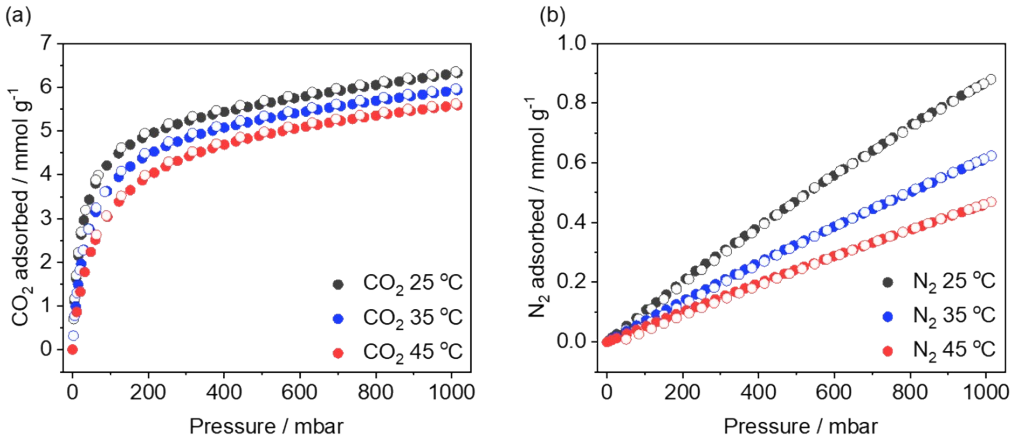

Figure S19. CO_2 and N_2 isotherms of Mg_2(dobpdc) at 298 K, 308 K, and 318 K. The close and open circles represent adsorption and desorption, respectively.

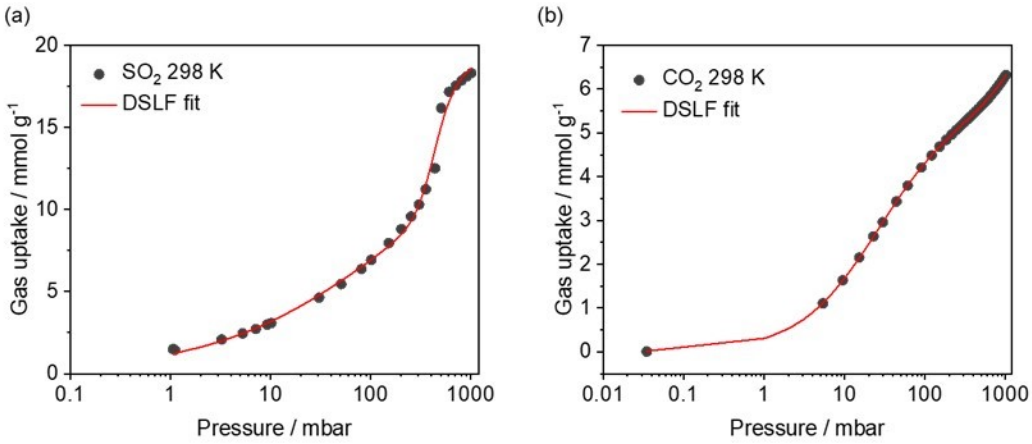

Figure S20. Dual site Langmuir Freundlich model (DSLF) fit of (a) SO_2 and (b) CO_2 isotherms at 298 K.

Table S6. Summary of Dual site Langmuir Freundlich model (DSLF) fit parameters.

Parameter	SO_2	CO_2
R^2	0.999524	0.999999
a_1	4.90346	11.9638
b_1	0.00219618	0.000100994
c_1	24.0065	0.986268
a_2	33.9159	5.34744
b_2	0.000379652	0.0413379
c_2	0.408879	0.899732

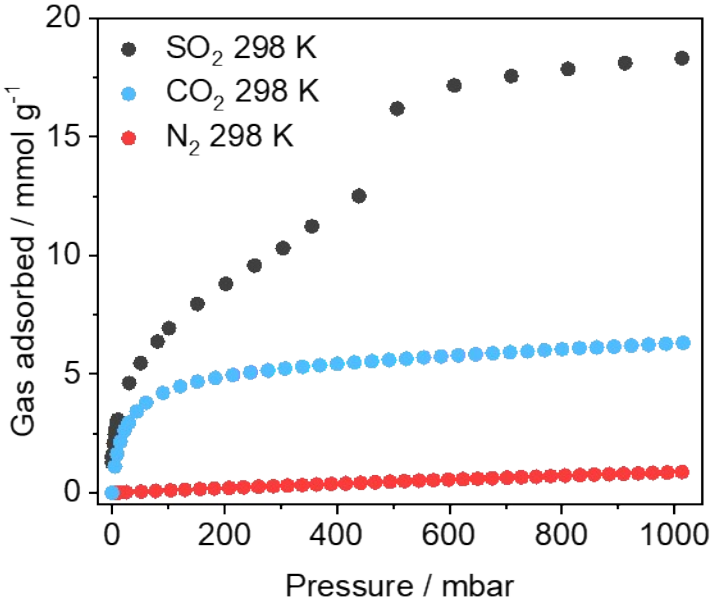

Figure S21. Comparison of SO_2, CO_2, and N_2 capacities at 298 K. It is worth noting that the SO_2 uptake in Mg_2(dobpdc) was higher at 298 K in the entire pressure range compared to those of the other gases.

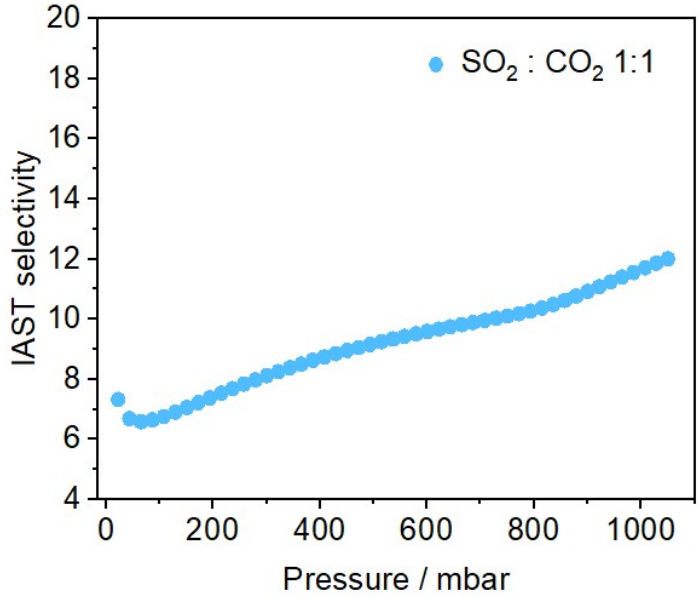

Figure S22. IAST selectivity of SO_2/CO_2 in an equimolar condition at 298 K.

Plots of Experimental Heat of Adsorption of CO_2 and N_2

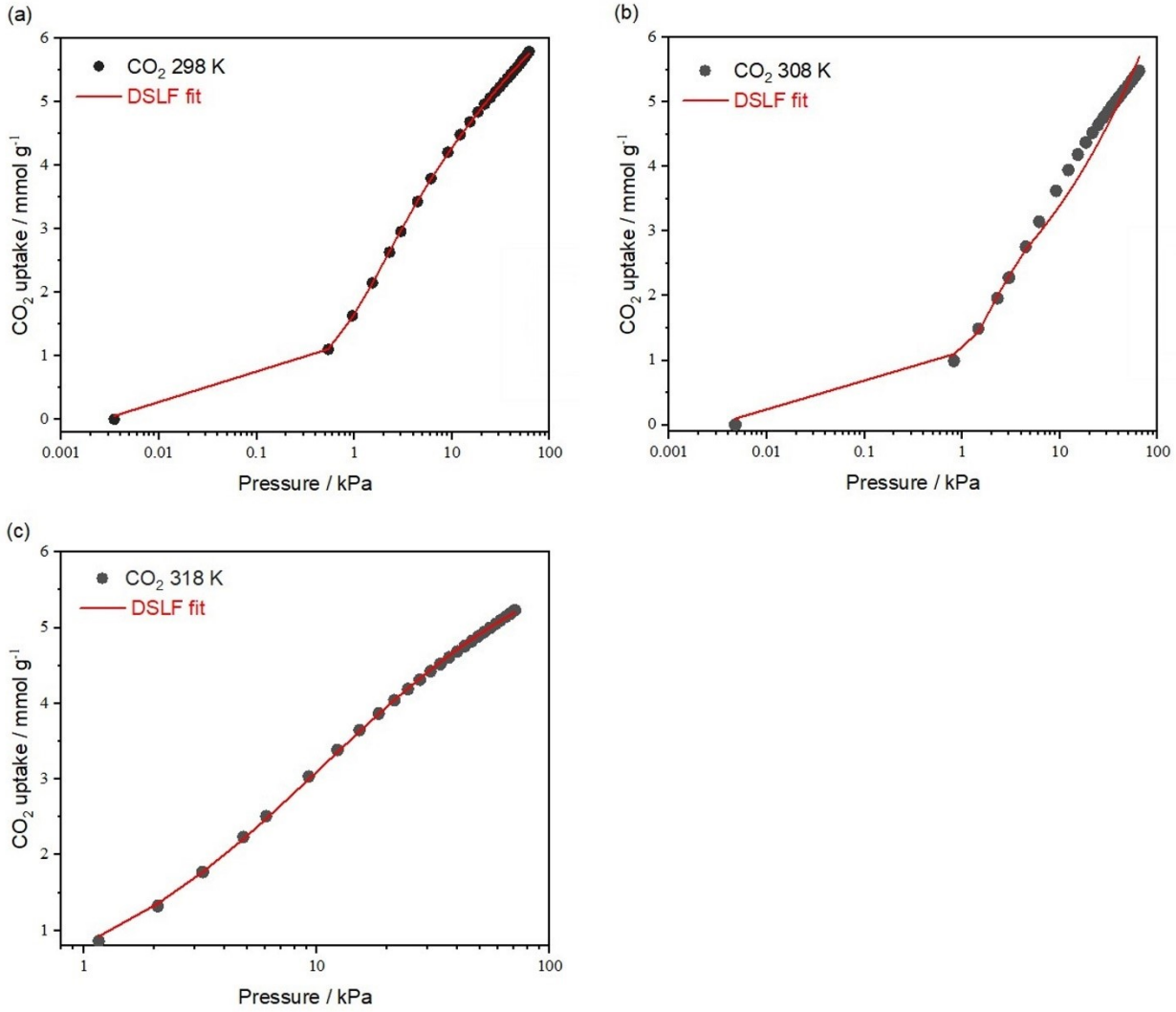

Figure S23. Dual site Langmuir Freundlich model (DSLF) fit of CO_2 isotherms at 298 K (a), 308 K (b), and 318 K (c).

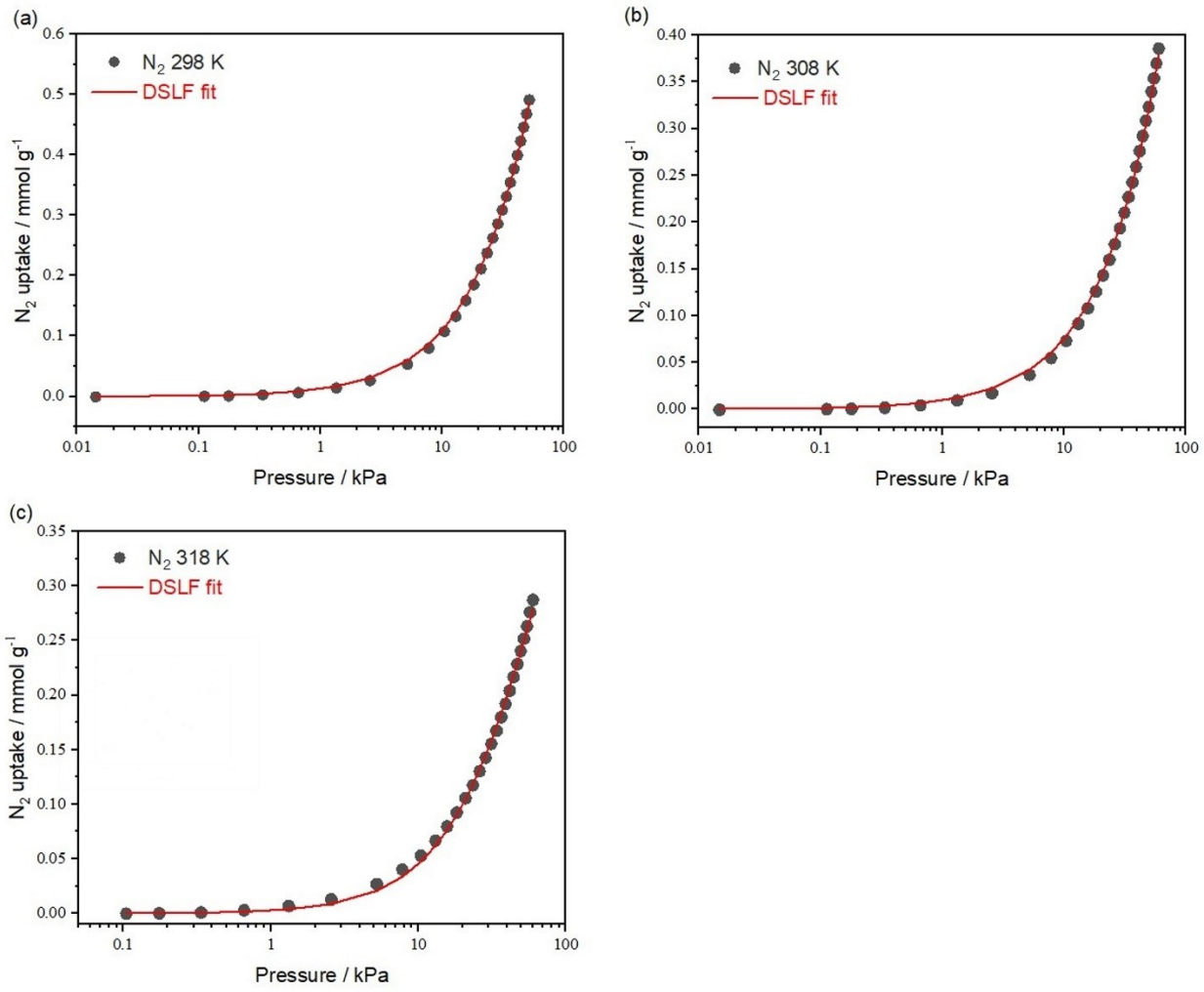

Figure S24. Dual site Langmuir Freundlich model (DSLF) fit of N_2 isotherms at 298 K (a), 308 K (b), and 318 K (c).

Fluorescence Spectroscopy

For the fluorescence experiments were carried in an Edinburgh Instruments FS5 Spectrofluorometer, coupled with the SC-10 solid-state sample holder.

For the emission experiments the solid samples were slightly ground in an agate mortar to homogenize the microcrystals. They were later packed into the quartz sample holders and positioned in the instrument. The activated samples were packed right after being taken out of the activation process and were left inside the fluorometer sample holder to measure over time, the last spectrum was analyzed 96

h later. Measurements were carried using an excitation wavelength of λ_{ex}= 320 nm, with an additional 330 nm high pass on the detector side to remove any remanent light from the excitation source. The measurements were collected with a step size of 1 nm, a dwell time of 0.50 s and two runs for every scan. The excitation bandwidth was set at 0.50 nm and the emission bandwidth for the detector at 3.00 nm.

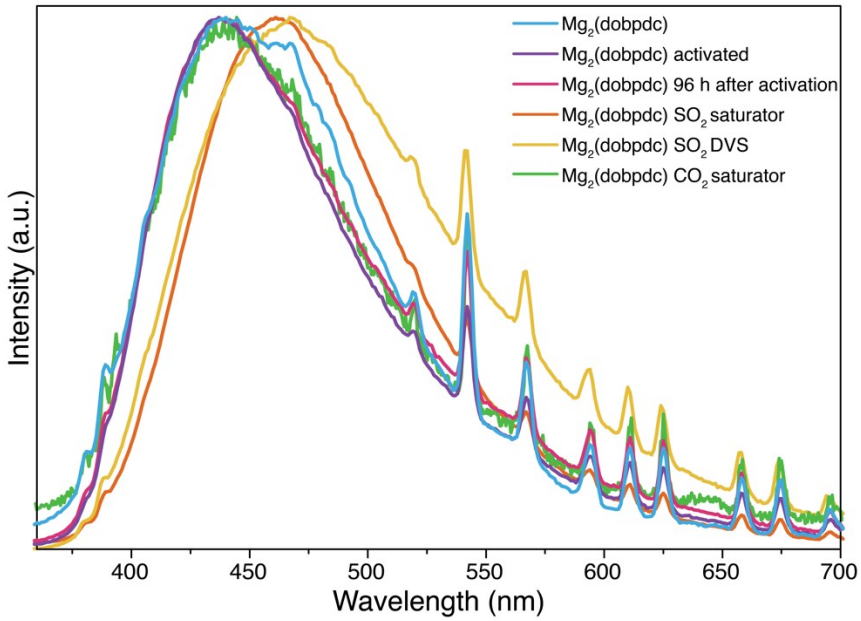

Figure S25. Normalised emission spectra of Mg_2(dobpdc) after exposure to different conditions.

REFERENCES

1. T. M. McDonald, W. R. Lee, J. A. Mason, B. M. Wiers, C. S. Hong, J. R. Long, Capture of Carbon Dioxide from Air and Flue Gas in the Alkylamine-Appended Metal–Organic Framework Mmen-Mg_2 (Dobpdc). *J. Am. Chem. Soc.* 2012, **134** (16), 7056. https://doi.org/10.1021/ja300034j.

2. K. I. Hadjiivanov, G. N. Vayssilov, Characterization of oxide surfaces and zeolites by carbon monoxide as an IR probe molecule. *Advances in Catalysis*, 2002, **47**, 307. https://doi.org/10.1016/S0360-0564(02)47008-3.

3. I. M. Hill, S. Hanspal, Z. D. Young, and R. J. Davis, DRIFTS of probe molecules adsorbed on magnesia, zirconia, and hydroxyapatite catalysts, *J. Phys. Chem. C* 2015, **119**, 9186. https://doi.org/10.1021/jp509889j.

4. C. Volkringer, H. Leclerc, J.-C. Lavalley, T. Loiseau, G. Férey, M. Daturi, and A. Vimont. Infrared Spectroscopy Investigation of the Acid Sites in the Metal–Organic Framework Aluminum Trimesate MIL-100(Al). *J. Phys. Chem. C* 2012, **11***6*, 5710. https://doi.org/10.1021/ja056906s.

5. H. Leclerc, A. Vimont, J.-C. Lavalley, M. Daturi, A. D. Wiersum, P. L. Llwellyn, P. Horcajada, G. Férey, and C. Serre, Infrared study of the influence of reducible iron(III) metal sites on the adsorption of CO, CO_2, propane, propene and propyne in the mesoporous metal–organic framework MIL-100. *Phys. Chem. Chem. Phys*., 2011, **1***3*, 11748. DOI https://doi.org/10.1039/C1CP20502A.

6. A. Vimont, J.-M. Goupil, J.-C. Lavalley, M. Daturi, S. Surblé, C. Serre, F. Millange, G. Férey, and N. Audebrand. Investigation of Acid Sites in a Zeotypic Giant Pores Chromium(III) Carboxylate. *J. Am. Chem. Soc*. 2006, **128,** 3218. https://doi.org/10.1021/ja056906s.

7. E. Martínez-Ahumada, M. L. Díaz-Ramírez, H. A. Lara-García, D. R. Williams, V. Martis, V. Jancik, E. Lima and I. A. Ibarra High and reversible SO_2 capture by a chemically stable Cr(III)-based MOF *J. Mater. Chem. A*, 2020, **8**, 11515. DOI https://doi.org/10.1039/C9TA13524C.

8. P. Li, Y. Xiang, V. H. Grassian, and S. C. Larsen, CO Adsorption as a Probe of Acid Sites and the Electric Field in Alkaline Earth Exchanged Zeolite Beta Using FT-IR and ab Initio Quantum Calculations. *J. Phys. Chem. B* 1999, **103***,* 24, 5058. https://doi.org/10.1021/jp9902093.

9. C. A. Fernandez, P. K. Thallapally, R. K. Motkuri, S. K. Nune, J. C. Sumrak, J. Tian, and J. Liu. Gas-induced expansion and contraction of a fluorinated metal–organic framework*. Cryst. Growth Des*. 2010, **10**, 1037. DOI: 10.1021/cg9014948.

10. L. Li, I. da Silva, D. I. Kolokolov, Xu. Han, J. Li, G. Smith, Y. Cheng, L. L. Daemen, C. G. Morris, H. G. W. Godfrey, N. M. Jacques, X. Zhang, P. Manuel, M. D. Frogley, C. A. Murray, A. J. Ramirez-Cuesta, G. Cinque, C. C. Tang, A. G. Stepanov, S. Yang and M. Schroder, Post-synthetic modulation of the charge distribution in a metal–organic framework for optimal binding of carbon dioxide and sulfur dioxide. *Chem. Sci*., 2019, **10**, 1472. https://doi.org/10.1039/C8SC01959B.

11. S. Yang, J. Sun, A. J. Ramirez-Cuesta, S. K. Callear, W. I. F. David, D. P. Anderson, R. Newby, A. J. Blake, J. E. Parker, C. C. Tang, M. Schröder, Selectivity and direct visualization of carbon dioxide and sulfur dioxide in a decorated porous host. *Nat. Chem*. 2012, **4**, 887. https://doi.org/10.1038/nchem.1457.

12. Brandt, A. Nuhnen, M. Lange, J. Möllmer, O. Weingart, C. Janiak Metal–Organic Frameworks with Potential Application for SO_2 Separation and Flue Gas Desulfurization. *ACS Appl. Mater. Interfaces* 2019, **11**, 19, 17350. https://doi.org/10.1021/acsami.9b00029.

13. N. Tannert, Y. Sun, E. Hastürk, S. Nießing, C. Janiak. A Series of new Urea-MOFs Obtained via Post-synthetic Modification of NH_2-MIL-101(Cr): SO_2, CO_2 and H_2O Sorption. *ZAAC* 2021, **11**, 1124. https://doi.org/10.1002/zaac.202100023.

14. M. Savage, Y. Cheng, T. L. Easun, J. E. Eyley, S. P. Argent, M. R. Warren, W. Lewis, C. Murray, C. C. Tang, M. D. Frogley, G. Cinque, J. Sun, S. Rudić, R. T. Murden, M. J. Benham, A. N. Fitch, A. J. Blake, A. J. Ramirez-Cuesta, S. Yang and M. Schröder, Selective Adsorption of Sulfur Dioxide in a Robust Metal–Organic Framework Material. *Adv.Mater.*2016, **28**, 8705. https://doi.org/10.1002/adma.201602338.

15. J. A. Zárate, E. Sánchez-González, D. R. Williams, E. González-Zamora, V. Martis, A. Martínez, J. Balmaseda, G. Maurin and I. A. Ibarra, High and energy-efficient reversible SO2 uptake by a robust Sc(iii)-based MOF. *J. Mater. Chem. A,* 2019, **7**, 15580. https://doi.org/10.1039/C9TA02585E.

16. K. Tan, P. Canepa, Q. Gong, J. Liu, D. H. Johnson, A. Dyevoich, P. K. Thallapally, T. Thonhauser, Jing Li, and Y. J. Chabal, Mechanism of Preferential Adsorption of SO_2 into Two Microporous Paddle Wheel Frameworks $M(bdc)(ted)_{0.5}$. *Chem. Mater.* 2013, **25**, 23, 4653. https://doi.org/10.1021/cm401270b.

17. Z. Zhu, P. Zhang, B. Li, S. Chen,Q. Deng, Z. Zeng ,J. Wang, S. Deng, Chemical immobilization of amino acids into robust metal–organic framework for efficient SO_2 removal. *AIChE J.* 2021, **67**, e17300. https://doi.org/10.1002/aic.17300.

18. S. Yang, L. Liu, J. Sun, K. M. Thomas, A. J. Davies, M. W. George, A. J. Blake, A. H. Hill, A. N. Fitch, C. C. Tang, M. Schröder, Irreversible Network Transformation in a Dynamic Porous Host Catalyzed by Sulfur Dioxide. *J. Am. Chem. Soc*. 2013, **135**, 4954. https://doi.org/10.1021/ja401061m.

19. Z. Zhu, P. Zhang, B. Li, S. Chen ,Q. Deng, Z. Zeng ,J. Wang, S. Deng, Chemical immobilization of amino acids into robust metal–organic framework for efficient SO_2 removal. *AIChE J.* 2021**, 67**, e17300. https://doi.org/10.1002/aic.17300.

20. X. Cui, Q. Yang, L. Yang, R. Krishna, Z. Zhang, Z. Bao, H. Wu, Q. Ren, W. Zhou, B. Chen and H. Xing, Ultrahigh and Selective SO_2 Uptake in Inorganic Anion-Pillared Hybrid Porous Materials. *Adv. Mater.* 2017**, 29**, 1606929. DOI: 10.1002/adma.201606929.

21. M. J. Yin, X. Hong X., Xue F. Feng, W. Y. Xu, R.Krishna, and F. Luo A Robust Cage-Based Metal–Organic Framework Showing Ultrahigh SO_2 Uptake for Efficient Removal of Trace SO_2 from SO_2/CO_2 and $SO_2/CO_2/N_2$ Mixtures*. Inorg. Chem.* 2021, **60,** 5, 3447. https://doi.org/10.1021/acs.inorgchem.1c00033.

22. Z. Chen, X. Wang, R. Cao, K. B. Idrees, X. Liu, M. C. Wasson, and O. K. Farha Water-Based Synthesis of a Stable Iron-Based Metal–Organic Framework for Capturing Toxic Gases. *ACS Materials Lett*. 2020, 2, **9**, 1129. https://doi.org/10.1021/acsmaterialslett.0c00264.

23. P. Brandt, S.-H. Xing, J. Liang, G. Kurt, A. Nuhnen, O. Weingart, and C. Janiak. Zirconium and Aluminum MOFs for Low-Pressure SO_2 Adsorption and Potential Separation: Elucidating the Effect of Small Pores and NH_2 Groups. *ACS Appl. Mater. Interfaces* 2021, **13***,* 29137. https://doi.org/10.1021/acsami.1c06003.

24. J. H. Carter, X. Han, F. Y. Moreau, I. da Silva, A. Nevin, H. G. W. Godfrey, C. C. Tang, S. Yang and M. Schröder Exceptional Adsorption and Binding of Sulfur Dioxide in a Robust Zirconium-Based Metal–Organic Framework*. J. Am. Chem. Soc.* 2018, **140**, 46, 15564. https://doi.org/10.1021/jacs.8b08433.

25. P. Brandt, A. Nuhnen, S. Öztürk, G. Kurt, J. Liang, and C. Janiak. Comparative Evaluation of Different MOF and Non-MOF Porous Materials for SO_2 Adsorption and Separation Showing the Importance of Small Pore Diameters for Low-Pressure Uptake. *Adv. Sustainable Syst*. 2021, **5**, 2000285.

26. Y. Sun, J. Liang, P. Brandt, A. Spieß, S. Öztürk and C. Janiak. Cucurbit[6]uril@MIL-101-Cl: loading polar porous cages in mesoporous stable host for enhanced SO_2 adsorption at low pressures. *Nanoscale*, 2021, **13**, 15952. https://doi.org/10.1039/D1NR04432J.

27. P. Brandt, A. Nuhnen, S. Öztürk, G. Kurt, J. Liang, and C. Janiak. Comparative Evaluation of Different MOF and Non-MOF Porous Materials for SO_2 Adsorption and Separation Showing the Importance of Small Pore Diameters for Low-Pressure Uptake. *Adv. Sustainable Syst*. 2021, **5**, 2000285.

28. K.Tan, S. Zuluaga, H. Wang, P. Canepa, K. Soliman, J. Cure, J. Li, T. Thonhauser, and Y. J. Chabal, Interaction of Acid Gases SO_2 and NO_2 with Coordinatively Unsaturated Metal Organic Frameworks: M-MOF-74 (M = Zn, Mg, Ni, Co). *Chem. Mater*. 2017, **29,** 4227. https://doi.org/10.1021/acs.chemmater.7b00005.

29. T. G. Glover, G. W. Peterson, B. I. Schindler, D. Britt, and O. Yaghi. MOF-74 building unit has a direct impact on toxic gas adsorption. *Chem. Eng. Sci.* 2011**, 66**, 163.https://doi.org/10.1016/j.ces.2010.10.002.

30. F. Chen, D. Lai, L. Guo, J. Wang, P. Zhang, K. Wu, Z. Zhang, Q. Yang, Y. Yang, B. Chen, Q. Ren, and Zo.i Bao Deep. Desulfurization with Record SO_2 Adsorption on the Metal−Organic Frameworks. *J. Am. Chem. Soc.* 2021, **143**, 9040. https://doi.org/10.1021/jacs.1c02176.

31. T. H. Y. Duong, T. N. Nguyen, H. T. Oanh, T. A. Dang Thi, L. N.Thuy Giang, H. T. Phuong, N. T. Anh, B. M. Nguyen, V. T. Quang, G. Truong Le, and T. V. Nguyen. Synthesis of Magnesium Oxide Nanoplates and Their Application in Nitrogen Dioxide and Sulfur Dioxide Adsorption. *Journal of Chemistry*, 2019, 4376429. https://doi.org/10.1155/2019/4376429

32. J. D.Gale, A. L. Rohl, The General Utility Lattice Program (<scp>GULP</Scp>). *Mol. Simul.* 2003, **29** (5), 291. https://doi.org/10.1080/0892702031000104887.

33. Sokolić, F.; Guissani, Y.; Guillot, B. Molecular Dynamics Simulations of Thermodynamic and Structural Properties of Liquid SO_2. *Mol. Phys.* 1985, **56** (2), 239. https://doi.org/10.1080/00268978500102291.

34. Rappe, A. K.; Casewit, C. J.; Colwell, K. S.; Goddard, W. A.; Skiff, W. M. UFF, a Full Periodic Table Force Field for Molecular Mechanics and Molecular Dynamics Simulations. *J. Am. Chem. Soc.* 1992, **114** (25), 10024. https://doi.org/10.1021/ja00051a040.

35. Willems, T. F.; Rycroft, C. H.; Kazi, M.; Meza, J. C.; Haranczyk, M. Algorithms and Tools for High-Throughput Geometry-Based Analysis of Crystalline Porous Materials. *Microporous Mesoporous Mater.* 2012, **149** (1), 134. https://doi.org/10.1016/j.micromeso.2011.08.020.

36. A. L. Myers and J. M. Prausnitz, Thermodynamics of mixed-gas adsorption, *AIChE J*, 1965, **11**, 121. https://doi.org/10.1002/aic.690110125-